Piezoelectric strain-mediated control of the tunnel magnetoresistance effect in magnetic tunnel junctions with a Co_2FeSi/V/PMN-PT multiferroic heterostructure

T. Usami,[1, 2] Y. Kubo,[2] K. Suzuki,[3, 4] S. Mizukami,[4, 5] and K. Hamaya[2, 1, a)]

[1)]*Spintronics Research Network Division, Institute for Open and Transdisciplinary Research Initiatives, The University of Osaka, Suita, Osaka 565-0871, Japan*

[2)]*Center for Spintronics Research Network, Graduate School of Engineering Science, The University of Osaka, Toyonaka, Osaka 560-8531, Japan*

[3)]*Department of Applied Physics, Graduate School of Engineering, Tohoku University, Sendai, Miyagi 980-8577, Japan*

[4)]*WPI Advanced Institute for Materials Research, Tohoku University, Sendai, Miyagi 980-8577, Japan*

[5)]*Center for Science and Innovation for Spintronics, Tohoku University, Sendai, Miyagi 980-8577, Japan*

(Dated: 17 June 2025)

Electric field (E) control of the tunnel magnetoresistance (TMR) effect is a key technology for reducing power consumption during data writing in spintronic memory devices. In this Letter, we explore E control of the TMR effect in magnetic tunnel junction (MTJ) devices with a Co_2FeSi/V/PMN-PT multiferroic heterostructure. By controlling the polarity of the applied E field to the multiferroic heterostructure, a repeatable and nonvolatile change in the TMR effect is achieved. The change in the TMR effect is strongly influenced by the microscopic domain structures in the Co_2FeSi layer after the application of a certain E. To obtain optimal changes, it is important to consider the control of the microscopic domain structure governed by the magnetoelectric effect in the multiferroic heterostructure.

[a)]hamaya.kohei.es@osaka-u.ac.jp

Magnetoresistive random-access memory (MRAM) is a promising candidate for next-generation nonvolatile memory technologies[1–4]. The memory cell in MRAM consists of a magnetic tunnel junction (MTJ)–a representative spintronic component composed of two ferromagnetic electrodes separated by an insulating tunnel barrier[5–7]. To write information, MRAM utilizes a spin-polarized current that passes through the MTJ[1–3]. However, this current-based writing operation induces Joule heating, leading to increased energy consumption during the write process[8]. To address this issue, electric-field (E)-controlled MRAM devices have been studied extensively[9–12]. Among several approaches, magnetoelectric random-access memory (MeRAM) has attracted attention because its predicted writing energy consumption is approximately 0.16 fJ/bit-significantly lower than that of conventional MRAM devices ($\sim$100 fJ/bit)[11,12]. In addition, the proposed device can simultaneously achieve room-temperature operation and high storage density. The key component of the writing scheme in MeRAM is a ferromagnetic/piezoelectric multiferroic heterostructure. This structure enables E-field control of the magnetization vector in the ferromagnetic layer at room temperature (RT) through a piezostrain-induced converse magnetoelectric (CME) effect[12–22]. Compared to other E-based approaches for controlling the magnetization vector – such as those employing ultrathin ferromagnetic layers[9,23,24]–multiferroic heterostructures have fewer limitations on the operating environment, particularly in terms of ferromagnetic layer thickness. To implement a multiferroic heterostructure in MTJ devices, both a large CME effect–with a CME coupling coefficient (α_{E}) exceeding 10^{-5} s/m–and nonvolatile memory operation are required. Experimental studies on MTJs with multiferroic heterostructures have used ferromagnetic CoFeB and piezoelectric $Pb(Mg_{1/3}Nb_{2/3})O_3$-$PbTiO_3$ (PMN-PT)[25–28]. However, the α_{E} value for CoFeB/PMN-PT was less than 10^{-5} s/m[29]. Recently, we discovered a multiferroic heterostructure with α_{E} exceeding 10^{-5} s/m, using ferromagnetic Co_2FeSi and piezoelectric PMN-PT.[30–32] In this Letter, we demonstrate E-field control of the TMR effect in MTJ devices with the Co_2FeSi/V/PMN-PT multiferroic heterostructure. By controlling the polarity of the applied E field, we achieve a repeatable and nonvolatile change in the TMR effect. This change is strongly influenced by the microscopic domain structures that appear in the Co_2FeSi layer following the application of a given E field. To achieve optimal changes in the TMR ratio, it is important to consider controlling the microscopic domain structure governed by the magnetoelectric effect in the multiferroic heterostructure.

Figure 1(a) shows a schematic of the stacked structure on a piezoelectric PMN-PT(011) substrate, fabricated using molecular beam epitaxy (MBE) and magnetron sputtering techniques.

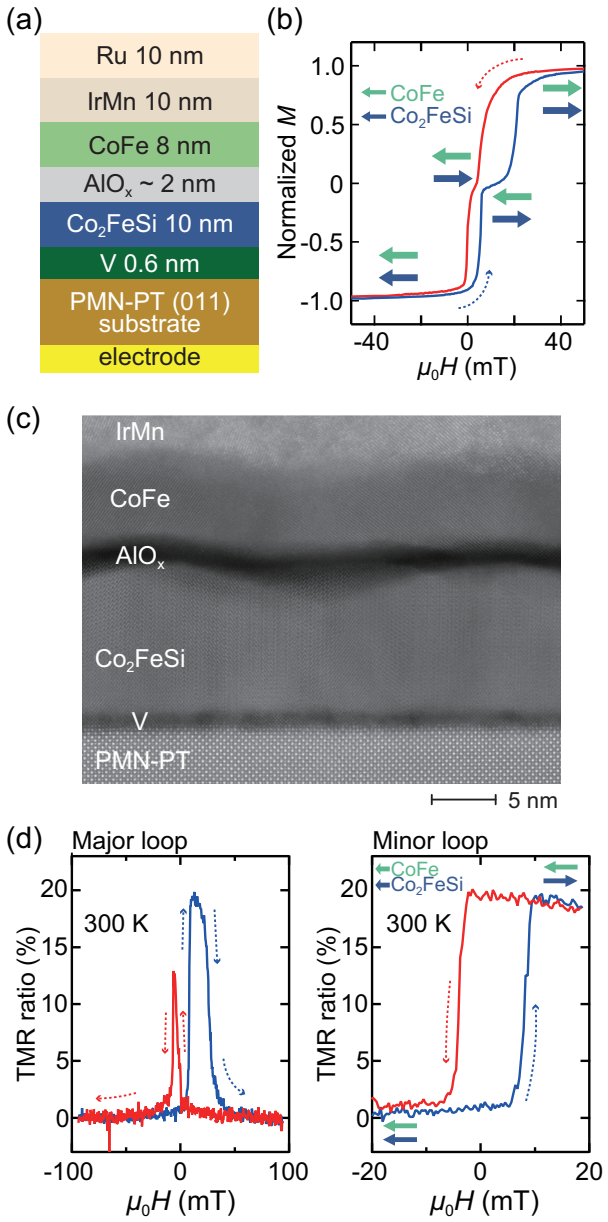

FIG. 1. (a) Stacking structure for MTJ devices. (b) Magnetization curve of the stacked films. H was applied along PMN-PT[01$\bar{1}$], and the red (blue) plot indicates the sweep from positive (negative) to negative (positive) fields. (c) A HAADF-STEM image of the stacked heterostructure. (d) Representative MR curve (left) and minor loop (right) for the MTJ device. The color code is the same as that in Fig. 1(b).

First, a 10-nm-thick Co_2FeSi layer was grown on the PMN-PT(011) substrate by MBE at 300°C, with the insertion of a vanadium (V) layer, which promotes the growth of a highly oriented Co_2FeSi layer[32]. After cooling to RT, a 1-nm-thick Al layer was deposited on the Co_2FeSi layer in the same MBE chamber, and an AlO_x layer was formed by *ex-situ* natural oxidation. Subsequently,

using magnetron sputtering, an 8-nm-thick CoFe layer was deposited on the AlO_x layer, followed by the deposition of IrMn and Ru layers. The samples were then annealed in a vacuum furnace at 250°C under a magnetic field to induce unidirectional anisotropy in the CoFe layer along the $[01\bar{1}]$ crystal axis of PMN-PT. In-plane magnetization curves of the stacked heterostructure were measured using a vibrating sample magnetometer (VSM) at RT. To characterize the TMR effect, spin-valve-type MTJs were fabricated using electron-beam lithography and Ar-ion milling. All TMR measurements were performed at RT.

Figure 1(b) shows the magnetization curve of the stacked heterostructure. Owing to the pinning effect induced by the antiferromagnetic IrMn layer, the magnetization curve exhibits both parallel (P) and antiparallel (AP) states. This characteristic is favorable for observing the TMR effect. A high-angle annular dark-field scanning transmission electron microscopy (HAADF-STEM) image of the stacked heterostructure is shown in Fig. 1(c). Although the AlO_x layer on top of the Co_2FeSi layer exhibits a roughness of approximately 1-2 nm, a several-nanometer-thick AlO_x tunnel barrier is clearly formed between the CoFe and Co_2FeSi layers. Representative MR curves of the major loop (left) and minor loop (right) at RT are shown in Fig. 1(d). In these measurements, in-plane external magnetic fields (H) were applied along the PMN-PT$[01\bar{1}]$ direction. The TMR ratio is defined as $(R_{\mathrm{H}} - R_{-40\mathrm{mT}})/R_{-40\mathrm{mT}} \times 100$, where R_{H} and $R_{-40\mathrm{mT}}$ are the junction resistances at a given H and at $H = -40$ mT, respectively. A field of -40 mT is sufficient to establish the parallel magnetization state. Clear MR changes due to magnetization switching were observed in the MTJ device fabricated on the Co_2FeSi/V/PMN-PT multiferroic heterostructure. Notably, both P and AP magnetization states were observed in the minor loop within an H range of ± 20 mT at room temperature. Correspondingly, two distinct MR states–low and high–were detected. This behavior demonstrates a clear nonvolatile memory effect, which provides the fundamental operation principle of MTJ-based memory devices. The observed TMR ratio of approximately 19% is lower than that reported in a previous study ($\sim$28%)[33], which we attribute to the roughness of the AlO_x tunnel barrier. Using these MTJ devices, we further investigated the effect of the electric field on the TMR response.

To detect the effect of E on the TMR ratio, we applied E to the PMN-PT substrate using the top Co_2FeSi and bottom Au electrodes, as shown in Fig. 2(a). Here, we focused on MR minor loop measurements to clearly observe the nonvolatile memory effect. Figure 2(b) shows an MR minor loop at the zero-field state $[E = 0(-)]$ after applying a negative E of -0.3 MV/m (sequence 1). To evaluate the TMR ratio modulation in the zero magnetic field, we define TMR(E)

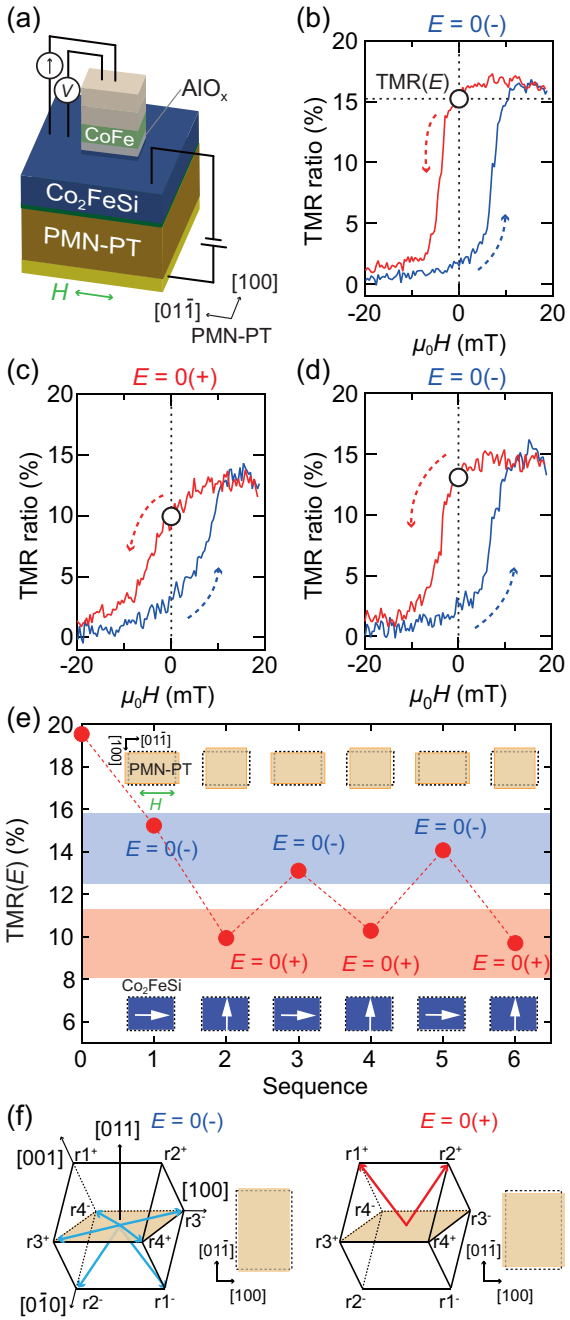

FIG. 2. (a) Schematic of the fabricated MTJ device. TMR minor loops for the MTJ device measured at (b) $E = 0(-)$ (sequence 1), (c) $E = 0(+)$ (sequence 2), and (d) $E = 0(-)$ (sequence 3) states, where the magnetic field was applied along PMN-PT[01$\bar{1}$]. (e) Repeated binary TMR changes by switching the sequence between $E = 0(-)$ and $E = 0(+)$. Here, the sequence 0 corresponds to the initial state displayed in Fig. 1 (c). The top and bottom insets present the ideal lattice deformation of the PMN-PT(011) plane and the magnetization vector of the Co_2FeSi layer, respectively, at $E = 0(-)$ and $E = 0(+)$. (f) Schematic illustration of the lattice deformation in the PMN-PT (011) plane and the corresponding polarization vectors at $E = 0(-)$ state (left) and $E = 0(+)$ state (right).

as the difference between the TMR ratio at $H = 0$ in the down-sweep curve (red) and at $H = -20$ mT. In this situation (sequence 1), the TMR(E) value decreased to approximately 15%. Next, after applying a positive E of + 0.3 MV/m, we measured the MR minor loop in the zero-field state [$E = 0(+)$], as shown in Fig. 2(c) (sequence 2). As a result, the TMR(E) value further decreased to approximately 10%. Notably, when we returned to the $E = 0(-)$ state by applying a negative E of -0.3 MV/m (sequence 3), the TMR(E) value increased to $\sim$13%, as shown in Fig. 2(d). Subsequently, we observed that the increase and decrease in the TMR(E) value could be repeatedly switched. A plot of the change in TMR(E) versus E application sequence is shown in Fig. 2(e). Sequence 3 [$E = 0(-)$] clearly shows an increase in TMR(E), indicating that the nonvolatile memory effect can be repeatedly controlled by switching the polarity of the applied E in the multiferroic heterostructure.

To understand the repeatable changes in the TMR effect, we first focused on the shape of the MR curves. By comparing the minor loop shapes shown in Fig. 2(b) and Fig. 2(c), we observe differences around zero magnetic field. This feature indicates that the magnetization vector of the bottom Co_2FeSi layer undergoes nonvolatile switching between the $E = 0(-)$ and $E = 0(+)$ states. We now explain why the magnetization vector of the bottom Co_2FeSi layer switches repeatedly. To this end, we tentatively consider the lattice deformation of the PMN-PT(011) plane at the $E = 0(-)$ and $E = 0(+)$ states[30]. Note that the charge-mediated contribution to magnetization control is considered negligible in our sample, as the thickness of the ferromagnetic Co_2FeSi layer (10 nm) is much greater than the typical screening length, which is on the order of only a few atomic layers.

The schematics in the top inset of Fig. 2(e) illustrate two distinct lattice deformation states of the PMN-PT(011) plane. Figure 2(f) provides the schematic illustration of the lattice deformation and corresponding polarization vectors in the PMN-PT(011) plane at the $E = 0(+)$ and $E = 0(-)$ states. It is well known that in rhombohedral PMN-PT, the polarization vectors can align along the eight body-diagonal directions of the pseudocubic unit cell[34–36]. At zero electric field, two representative domain configurations can be realized. One configuration, as shown in the right schematic, consists of polarization vectors pointing along the $r1^+$ or $r2^+$ directions, resulting in lattice elongation along the [100] direction[34]. The other configuration, illustrated in the left schematic, includes in-plane polarization vectors pointing along the $r3^\pm$ or $r4^\pm$ directions, leading to lattice elongation along the $[01\bar{1}]$ direction[35]. In the following, we discuss the relationship between the lattice deformation and the TMR(E).

In sequence 1, the PMN-PT(011) plane is likely elongated along the PMN-PT[01$\bar{1}$] direction, inducing strain-driven magnetic anisotropy along the same direction in addition to the intrinsic magnetic anisotropy of the Co_2FeSi layer.[30] Consequently, the magnetic easy axis (EA) of the Co_2FeSi layer remains aligned along PMN-PT[01$\bar{1}$], as shown in the bottom inset of Fig. 2(e). This direction matches that of the pinned CoFe magnetization. Consequently, a relatively high TMR(E) is observed in sequence 1 ($E = 0(-)$). However, in sequence 2 ($E = 0(+)$), compressive strain is expected along PMN-PT[01$\bar{1}$], which may cause the EA of the Co_2FeSi layer to rotate from PMN-PT[01$\bar{1}$] to PMN-PT[100]. Accordingly, a lower TMR(E) is observed in sequence 2. Based on these considerations, the repeatable and nonvolatile changes in the TMR ratio can be qualitatively explained by piezostrain-mediated reorientation of the EA in the Co_2FeSi layer of the multiferroic heterostructure, occurring between the two electric field states, $E = 0(-)$ and $E = 0(+)$.[30,32]

If ideal 90° switching of the magnetization vector in the Co_2FeSi layer occurred between the $E = 0(-)$ and $E = 0(+)$ states, the shape of the TMR curve at $E = 0(+)$ would resemble that of a magnetic hard axis (HA). However, as shown in Fig. 2(c), the curve still exhibits an EA-like shape. From the TMR(E) modulation shown in Fig. 4(e), the change in TMR between the $E = 0(-)$ and $E = 0(+)$ states is estimated to be approximately 40%. This value is smaller than the previously reported modulation of 55%[26], which was estimated using a similar method. For practical applications, enhancement of the TMR modulation is required to achieve substantial readout margins. To clarify the origin of this deviation, we investigated the magnetic domain structure in the Co_2FeSi layer using Kerr microscopy. For this purpose, we fabricated a patterned structure consisting of only a single free layer based on a Co_2FeSi/V/PMN-PT multiferroic heterostructure, as schematically illustrated in Fig. 3(a). Here, the Co_2FeSi layer was patterned into a rectangular structure with dimensions of 5×20 μm^2. The thicknesses of the V, Co_2FeSi, and AlO_x layers were 0.6, 10, and $\sim$ 2 nm, respectively. Figure 3(b) presents snapshots of the magnetic domain configurations at the $E = 0(-)$ and $E = 0(+)$ states under various magnetic fields H. In Fig. 3(b), the brighter contrast indicates that the magnetization in the region points to the right, while the darker contrast indicates that it points to the left. The white arrows show the estimated magnetization directions. In the top row of images corresponding to $E = 0(-)$, a uniform single-domain state was observed within the patterned region, and sharp magnetization reversal occurred upon sweeping H. This result confirms that the PMN-PT[01$\bar{1}$] direction aligns with the EA of the Co_2FeSi layer. In contrast, at $E = 0(+)$ (bottom images), complex multi-domain structures emerged during magnetization re-

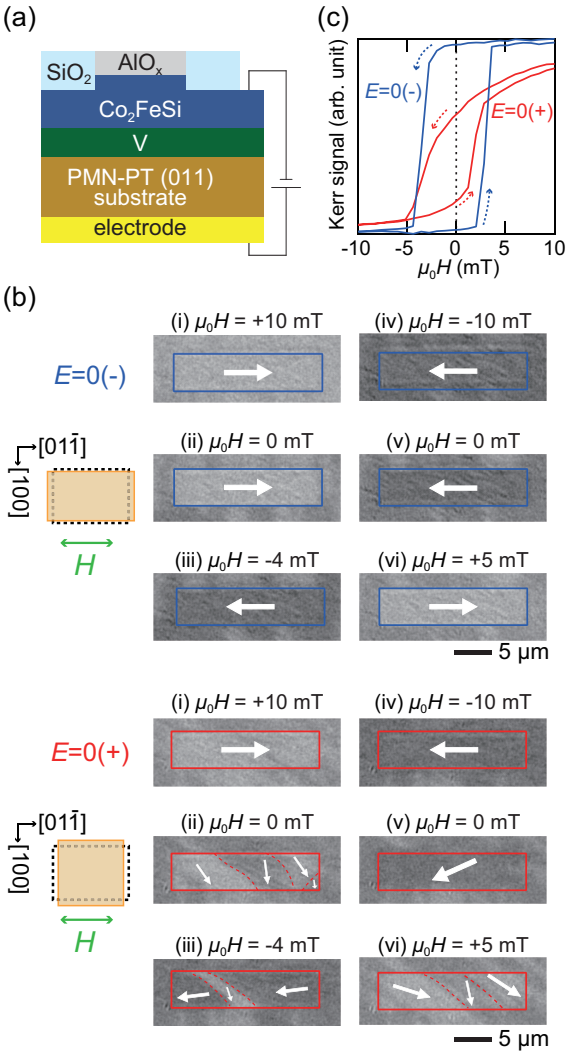

FIG. 3. (a) Schematic of a pattered structure for magnetic domain imaging. (b) Images of the magnetic domains at $E = 0(-)$ (top) and $E = 0(+)$ (bottom) states, where H was swept along PMN-PT[01$\bar{1}$]. The insets show the ideal lattice deformation of the PMN-PT(011) plane at $E = 0(-)$ and $E = 0(+)$. The white arrows indicate the magnetization direction. (c) A magnetization curve obtained from the domain image contrasts.

versal in the Co_2FeSi layer. That is, the multi-domains in the Co_2FeSi layer influence the magnetization switching at $E = 0(+)$ states. Figure 3(c) shows the magnetization curve obtained from the domain image contrasts in Fig. 3(b). Interestingly, we observe a strange magnetization curve with respect to the sweep direction of H at $E = 0(+)$, which is a possible origin of the presence of the EA-like shape of the TMR curve in Fig. 2(c), even at $E = 0(+)$. Therefore, it is quite important to control the microscopic magnetic domain configurations in Co_2FeSi/V/PMN-PT multiferroic

heterostructures to achieve more precise modulation of the TMR effect.

Finally, we discuss a method for controlling the microscopic magnetic domains in the Co_2FeSi/V/PMN-PT multiferroic heterostructure. When we enhanced the shape-induced magnetic anisotropy along the PMN-PT[100] direction and established a uniform in-plane piezoelectric domain state,[25] an ideal HA behavior was observed at the $E = 0(+)$ state. This outcome suggests that achieving a well-defined 90° switching of the magnetization vector in the Co_2FeSi layer is feasible, even for MTJs based on Co_2FeSi/PMN-PT multiferroic heterostructures.

In summary, we experimentally demonstrated repeatable and nonvolatile E-control of the TMR effect at RT by integrating a Co_2FeSi/V/PMN-PT multiferroic heterostructure into an MTJ device. Our findings highlight that the modulation of the TMR effect between the $E = 0(-)$ and $E = 0(+)$ states is significantly influenced by the microscopic magnetic domain structure in the Co_2FeSi layer. These results underscore the need to further optimize MTJ designs to effectively control magnetic domains via magnetoelectric coupling in multiferroic heterostructures.

This work was partially supported by JST CREST (Grant Numbers JPMJCR18J1 and JPMJCR17J5), JSPS KAKENHI Grant (Numbers JP21H05000, JP22H04964, JP22H05000, JP24H00034, JP24K17309), and the Spintronics Research Network of Japan (Spin-RNJ).

AUTHOR DECLARATIONS

CONFLICT OF INTEREST

The authors declare no conflict of interest.

DATA AVAILABILITY

The data supporting the findings of this study are available from the corresponding author upon reasonable request.

REFERENCES

[1]D. C. Ralph and M. D. Stiles, J. Magn. Magn. Mater. **320**, 1190 (2008).

[2]A. D. Kent and D. C. Worledge, Nat. Nanotechnol. **10**, 187 (2015).

[3]S. Ikegawa, F. B. Mancoff, J. Janesky, and S. Aggarwal, IEEE Trans. Electron Devices **67**, 1407 (2020).

[4]V. D. Nguyen, S. Rao, K. Wostyn, and S. Couet, npj Spintronics **2**, 48 (2024).

[5]S. Yuasa, T. Nagahama, A. Fukushima, Y. Suzuki and K. Ando, Nat. Mater. **3**, 868-871 (2004).

[6]S. S. P. Parkin, C. Kaiser, A. Panchula, P. M. Rice, B. Hughes, M. Samant and S.-H. Yang, Nat. Mater. **3**, 862-867 (2004).

[7]L. Li, K.-Y. Mak and Y. Zhou, Chinese Physics B **29**, 088701 (2020).

[8]F. Matsukura, Y. Tokura and H. Ohno, Nat. Nanotechnol. **10**, 209–220 (2015).

[9]T. Nozaki, T. Yamamoto, S. Miwa, M. Tsujikawa, M. Shirai, S. Yuasa and Y. Suzuki, Micromachines, **10**, 327 (2019).

[10]A. Fert, R. Ramesh, V. Garcia, F. Casanova and M. Bibes, Rev. Mod. Phys. **96**, 015005 (2024).

[11]J. M. Hu, Z. Li, L. Q. Chen, and C. W. Nan, Nat. Commun. **2**, 553 (2011).

[12]J.-M. Hu and C.-W. Nan, APL Mater. **7**, 080905 (2019).

[13]G. Venkataiah, Y. Shirahata, M. Itoh, and T. Taniyama, Appl. Phys. Lett. **99**, 102506 (2011).

[14]T. Taniyama, J. Phys: Condens. Matter **27**, 504001 (2015).

[15]J. M. Hu, L. Q. Chen and C. W. Nan, Adv. Mater. **28**, 15 (2016).

[16]J.-M. Hu, C.-G. Duan, C.-W. Nan, and L.-Q. Chen, npj Comput. Mater. **3**, 18 (2017).

[17]A. Molinari, H. Hahn, and R. Kruk, Adv. Mater. **31**, e1806662 (2019).

[18]M. Zheng, T. Usami and T. Taniyama, NPG Asia Mater. **13**, 7 (2021).

[19]W. Jahjah, J. Ph Jay, Y. Le Grand, A. Fessant, A. R. E. Prinsloo, C. J. Sheppard, D. T. Dekadjevi, and D. Spenato, Phys. Rev. Appl. **13**, 034015 (2020).

[20]V. Iurchuk, J. Bran, M. Acosta and B. Kundys, Appl. Phys. Lett. **122**, (2023).

[21]X. Li, H. Singh, J. Lin, S. Zhang, B. Yi, J. Chatterjee, Z. Xiao, S. Mondal, N. Tamura, R. N. Candler, L. You, J. Bokor, and J. Hong, npj Spintronics **2**, 34 (2024).

[22]T. Taniyama, Y. Gohda, K. Hamaya, and T. Kimura, Sci. Technol. Adv. Mater. **25**, 2412970 (2024).

[23]T. Maruyama, Y. Shiota, T. Nozaki, K. Ohta, N. Toda, M. Mizuguchi, A. A. Tulapurkar, T. Shinjo, M. Shiraishi, S. Mizukami, Y. Ando, and Y. Suzuki, Nat. Nanotechnol. **4**, 158 (2009).

[24]T. Nozaki, A. Kozioł-Rachwał, M. Tsujikawa, Y. Shiota, X. Xu, T. Ohkubo, T. Tsukahara, S. Miwa, M. Suzuki, S. Tamaru, H. Kubota, A. Fukushima, K. Hono, M. Shirai, Y. Suzuki and S. Yuasa, NPG Asia Mater. **9**, e451 (2017).

[25]A. Chen, Y. Zhao, Y. Wen, L. Pan, P. Li, and X.-X. Zhang, Sci. Adv. **5**, eaay5141 (2019).

[26]A. Chen, Y. Wen, B. Fang, Y. Zhao, Q. Zhang, Y. Chang, P. Li, H. Wu, H. Huang, Y. Lu, Z. Zeng, J. Cai, X. Han, T. Wu, X.-X. Zhang, and Y. Zhao, Nat. Commun. **10**, 243 (2019).

[27]Y. Zhang, W. Sun, K. Cao, X.-X. Yang, Y. Yang, S. Lu, A. Du, C. Hu, C. Feng, Y. Wang, J. Cai, B. Cui, H.-G. Piao, W. Zhao and Y. Zhao, Sci. Adv. **10**, eadl4633 (2024).

[28]W. Sun, Y. Zhang, K. Cao, S. Lu, A. Du, H. Huang, S. Zhang, C. Hu, C. Feng, W. Liang, Q. Liu, S. Mi, J. Cai, Y. Lu, W. Zhao and Y. Zhao, Sci. Adv. **10**, eadj8379 (2024).

[29]J. Wang, D. Pesquera, R. Mansell, S. van Dijken, R. P. Cowburn, M. Ghidini and N. D. Mathur, Appl. Phys. Lett. **114**, 092401 (2019).

[30]S. Fujii, T. Usami, Y. Shiratsuchi, A. M. Kerrigan, A. M. Yatmeidhy, S. Yamada, T. Kanashima, R. Nakatani, V. K. Lazarov, T. Oguchi, Y. Gohda, and K. Hamaya, NPG Asia Mater. **14**, 43 (2022).

[31]J. Okabayashi, T. Usami, A. Mahfudh Yatmeidhy, Y. Murakami, Y. Shiratsuchi, R. Nakatani, Y. Gohda, and K. Hamaya, NPG Asia Mater. **16**, 3 (2024).

[32]T. Usami, Y. Sanada, S. Fujii, S. Yamada, Y. Shiratsuchi, R. Nakatani, and K. Hamaya, Adv. Sci. **12**, 2413566 (2025).

[33]Y. Fujita, S. Yamada, Y. Maeda, M. Miyao, and K. Hamaya, Thin Solid Films **557**, 386 (2014).

[34]S. Zhang, Y. Zhao, X. Xiao, Y. Wu, S. Rizwan, L. Yang, P. Li, J. Wang, M. Zhu, H. Zhang, X. Jin and X. Han, Sci. Rep. **4**, 3727 (2014).

[35]M. Liu, T. Nan, J.-M. Hu, S.-S. Zhao, Z. Zhou, C.-Y. Wang, Z.-D. Jiang, W. Ren, Z.-G. Ye, L.-Q. Chen and N. X. Sun, NPG Asia Mater. **8**, e316-e316 (2016).

[36]M. Zheng, X.-K. Xu, H. Ni, Y.-P. Qi, X.-M. Li and J. Gao, Appl. Phys. Lett. **112**, (2018).